Modeling and Analysis of the Arc Light Spectrum in GMAW

The radiation produced during gas metal arc welding (GMAW) was analyzed by mathematically modeling both single and multiple wavelengths

BY M. S. WEGLOWSKI

ABSTRACT. The light from the welding arc can be seen as a signal carrying essential information about the welding process, and it has been exploited in the monitoring of the welding process. This paper analyzes the radiation of gas metal arc welding (GMAW) by mathematically modeling both single and multiple wavelengths. To this end, the methodology used to calculate the spectrophotometer spectral response is presented. The range of the tested wavelengths has been limited to visible radiation of the welding arc in the range of 480–700 nm. The conditions of arc burning were modified by changing the welding parameters. During experiments, the welding current changed in the range of 104–235 A. The spectrum of the radiation of the welding arc has been analyzed. The distribution of the electric arc light emission has also been examined. To characterize the single emission line, central wavelength, intensity, and full width at half maximum (FWHM), are needed. To this end, a mathematical model has to be used to approximate the real shape for a single wavelength with sufficient accuracy. Three fitting functions — Lorentz, Gauss, and Voight — were investigated as the methods to model the spectrum distribution. The fitting for both single and multiple wavelengths has been carried out mathematically and the best result was achieved with the Lorentz function.

Introduction

Gas metal arc welding (GMAW) is the most widely used process in robotic welding for mass production of welded components. It employs a continuous, consumable, solid wire electrode and an externally supplied shielding gas. The consumable wire electrode produces an arc with the workpiece and provides filler to the weld joint. The wire is fed to the arc by an automatic wire feeder, in which both push and pull modes have been employed, depending on the wire composition, diameter, and welding application (Ref. 1).

One of the major goals of process monitoring in welding is to ensure that the required welding parameters are being applied to make quality welds. If abnormal welding parameters are detected, the resultant segment of welds may be examined using more precise methods (Refs. 2–6). This would help reduce the need for strict/expensive process controls and reduce extensive use of costly postnondestructive examination (NDE) for all welds. To realize this goal, the monitoring devices are required to be fully automatic and the data analysis of sensed signals including welding parameters and the signal generated from the welding arc need to be optimized. In addition, the monitoring devices must also incorporate the criteria so that they can judge if the welds are acceptable or need additional examinations/repairs (Ref. 7).

Monitoring of welding processes can be divided into traditional and nontraditional methods (Ref. 8). The traditional methods are based on monitoring of electrical and other direct welding parameters (Refs. 9–12). The nontraditional ones use many different signals; for example, X-ray radiation (Ref. 13), infrared (IR) and ultraviolet (UV) emission (Ref. 14), ultrasonic wave (Ref. 15), acoustic emission (Ref. 16), and sound (Refs. 17, 18) to analyze and detect the process.

Traditional methods have been effectively used in welding process monitoring and control with success. For example, measurements of welding current and arc voltage can be used to estimate the stability of welding processes, especially with advanced methods of signal analysis and AI methods (Refs. 19–22). The so-called "through the arc sensing," which is based on measurement and analysis of welding current and arc voltage, is a widely used traditional method that has been accepted as one of the effective methods for weld joint tracking. The synergic control of GMAW machines (Ref. 23) is also based on measurements of current and arc voltage. One interesting case where online control of weld quality is based on the characteristics of welding arc signal is narrow groove GMAW with electromagnetic arc oscillation (Ref. 24). The relatively complex plasma arc welding process also can be monitored by using the electrical signal from the pilot arc (Ref. 25). In addition, traditional methods are also useful in the welding process in the form of surface impurities and insufficient shielding in GMAW (Ref. 12).

While the traditional methods have the advantage of being low cost and have achieved many successes as mentioned previously, many issues may require use of more signals than the welding current, arc voltage, and other direct welding parameters. For example, monitoring and control of weld penetration are important issues in welding (Ref. 26) that may require use of nontraditional methods. Real-time vision systems take the lead in the nontraditional monitoring methods especially for robotic welding applications (Ref. 27). The charge-coupled device (CCD) video cameras that can be used with fast algorithms can give us in-real-time estimates of stability of the process and quality of welds, for example, depth of penetration (Ref. 28). However, the investment for nontraditional methods is typically high. Cost-effective nontraditional methods such as arc light radiation monitoring,

KEYWORDS

Arc
Arc Light Emission
Spectrum
Spectrophotometer Card
GMAW

*M. S. WEGLOWSKI (*Marek.Weglowski@is.gliwice.pl*) is with the Polish Institute of Welding, Gliwice, Poland.*

which can measure and analyze the intensity of the whole range of the arc light spectrum or intensity of a single emission line (Refs. 29–37), are thus desired.

The arc light occurs in all arc welding methods. In most cases it is visible and can create a hazard for welders' eyes (Refs. 38–40), but it is also one of the signals emitted in the course of welding and can be utilized as a carrier of information about the welding process.

Following are some of the sources of visible radiation in the welding arc: the arc column, the regions close to the electrodes, liquid metal transported across the welding arc, the molten pool, the heated region of base material around the molten pool, and heated end of the electrode wire. Hot slag may also be a source of radiation. The range of length of the emitted light waves and their spectral composition depend on the welding parameters, the atmosphere in which the arc glows, and the kind of base and consumable material, as well as on several other parameters. The intensity of radiation produced by the welding arc is a function of the welding process itself and of the welding variables (Refs. 39–40).

Measurements and the analysis of the arc light emission are used in investigations of the welding process (Refs. 29–37). During the investigations, the following characteristics were specified: temperature distribution in the arc, temperature of the drops of liquid metal, amount of hydrogen in the gaseous shield of the welding arc, and temperature of the weld pool. The investigations were also conducted to calculate the mean temperature of the welding arc (Ref. 41). The analysis of the arc light emission may help to develop the technique of taking photographs of the welding arc (Ref. 42). Investigations on the visible radiation of the GMA method also help to monitor the way in which the metal is transferred through the arc (Ref. 33). Optical methods also are applied to scan the length of the welding arc in the gas metal arc (Refs. 35, 36) and the gas tungsten arc methods (Refs. 29–32). This signal is much more sensitive to the changes in the welding conditions and should be used as a tool for monitoring the GTAW process (Ref. 29).

This paper describes the acquisition and analysis of the arc light spectrum and the correlation of data to the welding parameters: welding current and arc voltage. The shape of the spectrum was modeled with three mathematic functions: Lorentz, Gauss, and Voight.

Experiment

Figure 1 shows the schematic layout of the experimental GMAW setup. A

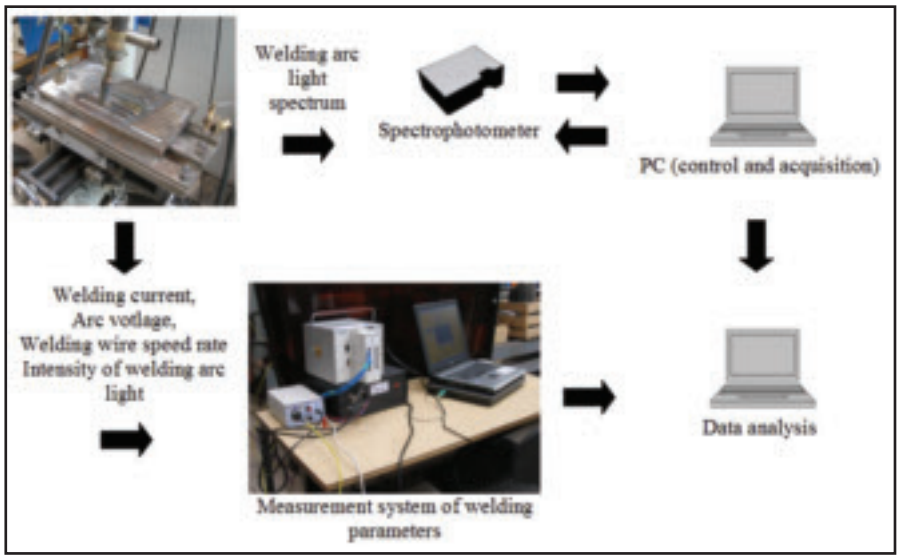

Fig. 1 — Experimental setup with measurement system.

welding power supply (OZAS MAGOMIG550) equipped with a ZP-15 OZAS wire feeder was used. The power supply was operated in constant voltage mode. The experiments were carried out on an automated welding table that was composed of a mechanism of longitudinal motion, a control system of longitudinal motion, and a manual mechanism of lateral motion. The torch was fixed on a set of supports with a horizontal and vertical adjustment. This allowed accurate setup of the distance between welding gun and plate. The torch was fixed and positioned normal to the plate surface for the bead-on-plate welds. The plate was fixed to the table by clamps, and the table was power driven by feed screw with continuously controlled travel speed. The filler metal used was SG2 (equivalent to AWS A5.18-79: ER70S-6) wire with a diameter of 1.2 mm (0.047 in.). The base metal was mild steel S255 (EN 10025) of 20 mm (0.78 in.) thickness. The shielding gas was 82% argon, 18% CO_2 with a flow rate of 16 L/min (0.56 ft^3/h). The welding parameters, which were choosen experimentally to produce well-shaped welds, are shown in Table 1.

The purpose of the investigation was to find the influence of welding current on the light spectrum radiation during GMAW. Experiments were performed on clean plates. The bead-on-plate welds produced are shown in Fig. 2. The welding parameters are given in Table 2. The macro-

Table 1 — Experimental Conditions Used

Parameter	Welding Conditions
Shielding Gas	Argon – 18% CO_2
Flow Rate of Shielding Gases (L/min)	16
Welding Current (A)	104, 130, 189, and 235
Contact Tube-to-Work Distance (mm)	20
Travel Speed (cm/min)	27, 30, 35, and 40
Electrode Type	ER70S-6
Electrode Diameter (mm)	1.2

Table 2 — GMA Welding Parameters

S.N.	Welding Current I (A)	Arc Voltage (V)	Welding Speed (cm/min)	Heat Input (kJ/cm)
I	104	16.5	27	4.8
II	130	18	30	6.5
III	189	21.1	35	11.0
IV	235	25.5	40	16.7

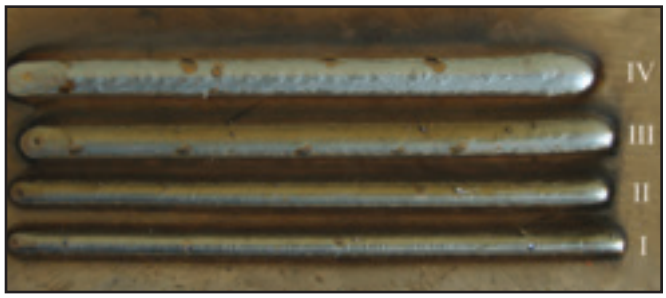

Fig. 2 — GMAW beads made in Ar + CO_2 shielding gas with the different welding parameters shown in Table 2.

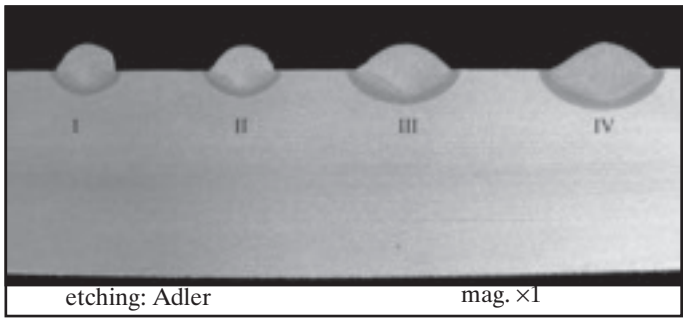

Fig. 3 — Macroscopic examination of padding welds. The welding parameters are presented in Table 1.

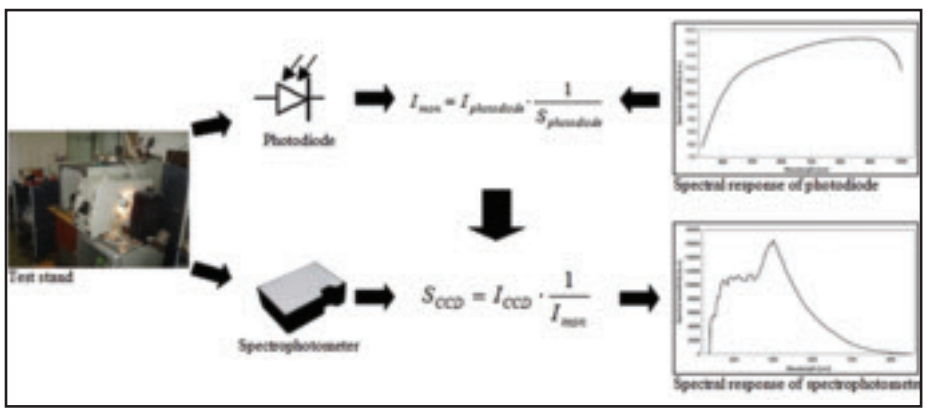

Fig. 4 — Methodology to calculate spectral response characteristic of spectrophotometer.

scopic examination of padding welds is shown in Fig. 3.

Measurement System

The measuring system consisted of the welding current and voltage transducers, an electro-optical converter, a data acquisition card, and a PC. The beam to be analyzed was fed into the electro-optical converter by means of standard fiber optics. The electrical signal corresponds to the visible light intensity. Signals from the welding circuit were recorded on the PC through the data acquisition card NI DAQ 6036.

A spectrophotometer card PCI 2000 ISA-A, which was designed for remote fiber spectroscopy in the visible spectral range of 340 to 860 nm, was used in the investigation. The CCD detector was a line scan array of 2048 pixels. The specification of the spectrophotometer card is given in Table 3.

Before the spectrum analysis of the welding arc emission can be performed, the spectral response characteristic of the spectophotometer card needs to be calculated. To this end, it was necessary to design and build a stand to measure light emission. This stand includes a monochromator SPM2, an ammeter K 485, a photodiode HAMAMATSU, and a spectrophotometric card PCI 2000 ISA-A. For data acquisition and control of the stand, LabView software was used. The methodology for calculating the spectral response characteristic of the spectrophotometer card is shown in Fig. 4, where

I_{mon} is the intensity of light from the monochromator (photon/(m^2s)),

$I_{photodiode}$ is the intensity measure by photodiode (photon/(m^2s)),

$S_{photodiode}$ is the spectral response of the photodiode (a.u.),

S_{CCD} is the spectral response of the spectrophotometer (a.u.),

I_{CCD} is the intensity measure by spectrophotometer (a.u.).

The influence of the spectral response of the spectrophotometer card on the results of the measurement of the spectrum of the welding arc light emission is demonstrated in Fig. 5. The measurements were carried out with a welding current of I = 130 A, arc voltage of U=18 V, and Ar-CO_2 as the shielding gas. In Fig. 5, one can easily see that the spectral response of the spectrophotometer card does affect the measurement of the arc light spectrum significantly. The shape of the measured spectrum of the welding arc substantially changed after calculation of the original date with spectrophotometer characteristic.

Table 3 — Data of Spectrophotometer Card

Detector	2048-element linear silicon CCD array
CCD Elements	2048 elements - 14 µm × 200 µm per element
Well Depth (600 nm)	160,000 photons
Sensitivity (estimated)	86 photons/count
	2.9 × 10-17 joule/count
	2.9 × 10-17 watts/count (for 1-s integration)
Detector Range	200–1100 nm
Useable Range	200–850 nm
Integration Time	3 ms to 60 s (with 1 MHz A/D converter)

Results and Discussion

The purpose of this study was to find the influence of the welding current on the light emission during GMAW. To that end, beads on plate were made on mild steel. The entire arc column was analyzed as a single object. Figure 6 shows the arc spectrum obtained in the range of 480–700 nm at the welding current in the range of 104–235 A and 82% Ar-18% CO_2 as the shielding gas. The graph is presented in a logarithmic scale.

In the previous studies, line spectra were considered as a line without width and distribution. To more accurately describe spectra lines, the author proposes to consider them as distributions that have a center wavelength and wavelength width. To this end, three functions — Gaussian, Lorentz, and Voight — were considered and the least square method and Levenberg-Marquardt algorithm

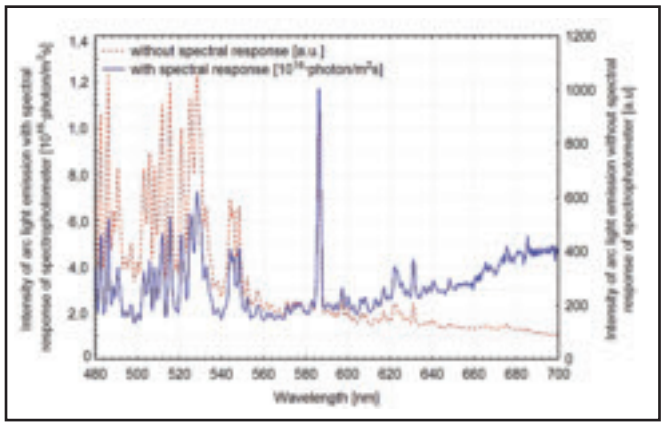

Fig. 5 — Influence of spectral response of spectrophotometer on results of measurement of spectrum arc light emission. I = 130 A, U = 18.0 V, Ar + CO_2.

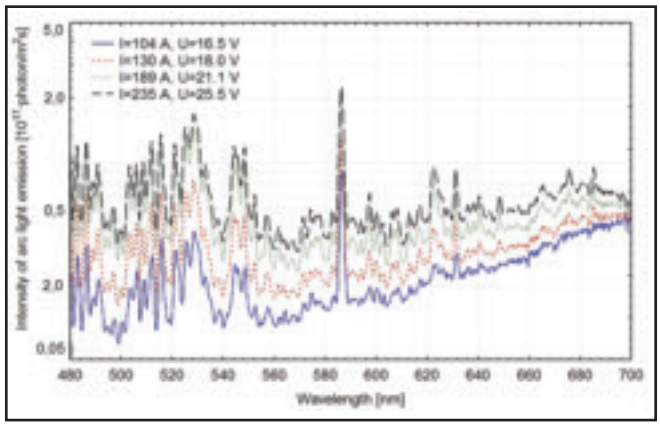

Fig. 6 — Effect of the welding current on the arc light spectrum. The welding current in the range of 104–235 A, Ar + CO_2 as the shielding gas, wavelength in the range of 480–700 nm. Logarithmic scale.

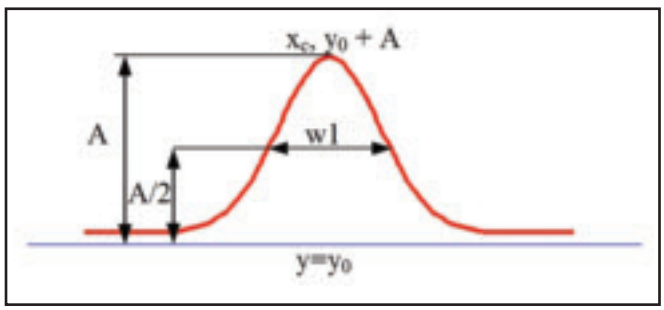

Fig. 7 — Characteristic qualities for the Gaussian function.

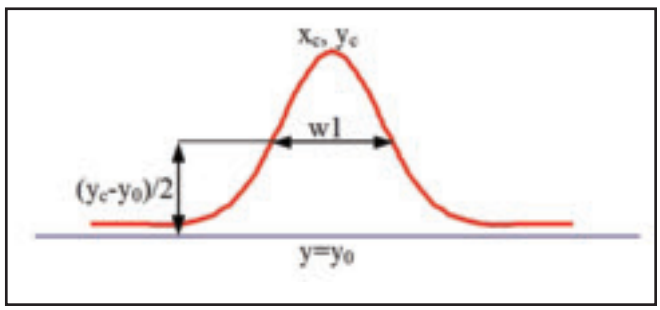

Fig. 8 — Characteristic parameters for the Lorentz function.

were used to identify the model parameters. Fitting can and has been carried out simultaneously also for multi-emission lines. All results were compared with the measurements.

For the Gaussian function, the profile of the single wavelength can be expressed as

$$y = y_0 + Ae^{\frac{\left(x - x_c\right)^2}{2w^2}} \quad (1)$$

where A = amplitude, w = width, x_c = center of the wavelength.

The width of the wavelength is calculated as

$$w = \frac{w\ l}{2\sqrt{ln\left(4\right)}} \quad (2)$$

The characteristic parameters of the Gaussian function are shown in Fig. 7. The initial conditions used for calculation were offset $y_0 = 0$, center $x_c = 0$, width wl = 1, and amplitude A = 10.

For the Lorentz function, the profile is described by

$$y = y_0 + \frac{2A}{\pi}\frac{w\ l}{4\left(x - x_c\right)^2 + w\ l^2} \quad (3)$$

Figure 8 shows the characteristic qualities of the Lorentz function.

The maximum value for the center of the wavelength can be expressed as

$$y_c = y_0 + \frac{2A}{w\ l \cdot \pi} \quad (4)$$

The initial conditions used for calculation were offset $y_0 = 0$; center $x_c = 5$; width wl = 2; and amplitude A=1.

Finally, for the Voight function the following function was used:

$$y = y_0 + A\frac{2ln2}{\pi^{3/2}}\frac{w_L}{w_G^2} \int_{-\infty}^{\infty} \frac{e^{-1^2}}{\left(\sqrt{ln2}\frac{w_L}{w_G}\right)^2 + \left(\sqrt{4ln2}\frac{x - x_c}{w_G} - t\right)^2} dt \quad (5)$$

where w_L is Lorentz width of emission line and w_G is Gaussian width of emission line. Figure 9 shows the characteristic parameters of the Voight function.

The line profiles of the wavelength 586.27 nm fitted using three different functions are compared with measurements as shown in Fig. 10 and for the multi-emission lines in Fig. 11. Table 4 gives the fitting results for all single lines in the range of 480 to 700 nm for welding current I = 130 A, arc voltage U = 18.0 V, and Ar + CO_2 shielding gas. The assigned in principle were carried out based on the National Institute of Standards and Technolgy database (Refs. 43–45).

As can be seen, the Lorentz function provides better fitting for the single line. Hence the Lorentz function was chosen for subsequent calculations.

The spectrum of the GMAW arc is composed of a continuous background spectrum that follows the blackbody radiation law with discrete lines superimposed on it. The shape of the discrete lines is modified by two major causes, namely collision line broadening and Doppler broadening (Ref. 46). Collision broadening is caused by the relatively high pressure (~ 1 bar) of the arc plasma. This pressure

Table 4 — Results of Fitting Single Emission Line and Assigned the Elements to Wavelengths

No.	Real Wavelength (nm)	Intensity (10^{16} photon/m^{2}s)	Lorentz	Width (nm)	Gauss	Voight	Fitting Elements to Wavelength (Refs. 43–45)
1	478.22	3.30	478.12±0.06	1.93±0.26	478.10±6.03	478.29±0.61	Mn I
2	479.90	4.32	479.97±0.03	1.25±0.10	480.35±7.42	479.69±159.60	Fe XVI
3	482.57	5.39	482.65±0.03	1.36±0.21	482.56±2.11	482.42±3.97	Mn I
4	486.25	6.06	486.22±0.02	1.22±0.10	486.25±0.44	486.18±0.47	Fe V
5	488.59	3.16	488.60±0.08	1.25±0.30	488.81±23.65	488.78±6.68	Fe I
6	490.93	3.97	490.93±0.05	1.94±0.27	490.91±6.40	490.87±4.70	Fe I
7	496.92	2.35	496.96±0.02	3.60±1.03	496.89±8.35	496.75±14.77	Fe I
8	500.25	1.94	500.07±0.02	3.24±0.31	500.06±6.52	499.85±12.77	Fe I
9	503.24	3.80	503.27±0.01	2.48±0.13	503.26±0.36	503.26±0.41	Fe XVI
10	505.90	4.26	505.86±0.07	1.33±0.59	505.84±33.49	505.74±14.85	Fe I
11	508.55	3.99	508.50±0.02	1.66±0.25	508.44±9.00	508.51±4.37	Fe I
12	511.87	5.45	511.57±0.07	2.64±0.78	511.62±0.86	511.44±1.78	Mn I
13	515.51	6.17	515.59±0.02	1.54±0.12	515.61±0.16	515.62±0.36	Fe I
14	521.13	5.42	521.12±0.09	1.28±0.48	521.24±1.78	521.12±2.43	Mn XX
15	525.09	6.32	525.60±0.09	6.57±0.63	525.59±0.77	525.59±0.81	Fe I
16	528.39	7.29	528.70±0.05	4.07±0.22	528.79±0.16	528.13±2.88	Fe I
17	532.99	3.84	533.11±0.14	1.96±0.56	532.52±175.40	532.40±168.87	Fe I
18	544.15	4.77	544.00±0.06	1.41±0.25	544.33±13.01	543.92±9.07	Fe IV
19	545.46	4.46	545.68±0.15	2.87±0.45	545.22±6.76	546.37±38376.0	Fe I
20	548.41	4.77	548.22±0.05	1.67±0.31	548.22±2.06	547.91±6.29	Mn XXI
21	552.33	2.67	552.22±0.04	2.05±0.40	552.21±11.67	551.99±33.06	Fe IV
22	557.22	2.35	557.24±0.02	2.62±0.16	557.21±0.47	557.21±0.16	Fe I
23	561.78	2.04	561.90±0.03	2.15±0.26	561.95±2.34	561.91±1.09	Mn XIX
24	563.73	2.00	563.90±0.04	2.09±0.76	563.77±265.54	563.69±690.32	Fe I
25	566.98	1.92	567.12±0.05	2.25±0.61	567.07±2.96	566.97±10.91	Fe XVI
26	571.20	2.34	571.45±0.06	2.84±0.88	571.45±1.99	571.45±2.36	Mn XX
27	574.12	2.40	574.28±0.41	1.61±0.25	574.42±27.06	574.37±13.08	Fe I
28	576.38	2.43	576.31±0.06	1.37±0.29	—	—	Fe I
29	577.68	2.38	577.89±0.08	2.01±0.36	—	—	Fe I
30	586.27	12.7	586.26±0.01	1.71±0.09	586.29±0.06	585.99±1.29	Fe XXI
31	590.26	2.41	590.82±0.07	7.21±0.41	590.82±0.22	590.29±7.73	Fe I
32	594.12	2.40	594.15±0.03	1.26±0.33	594.14±76298.79	593.99±118.29	Fe I
33	597.34	3.09	597.26±0.03	1.50±0.19	597.34±3.41	596.99±3.24	Fe I
34	599.90	2.71	599.95±0.05	2.16±0.27	599.90±606.96	599.75±77.93	Fe III
35	602.79	1.33	602.72±0.08	3.48±0.44	—	—	Fe III
36	606.31	2.64	606.19±0.03	1.28±0.13	—	606.07±12.31	Fe IV
37	608.23	2.69	608.22±0.04	2.15±0.16	608.40±0.67	608.11±119.25	Fe IV
38	613.02	2.62	613.10±0.05	1.99±0.60	613.02±1414.99	612.87±35.56	Fe I
39	617.16	3.13	617.11±0.06	2.10±0.45	617.19±2.63	617.18±2.01	Fe II
40	622.25	4.03	622.95±0.08	6.66±3.58	—	—	Fe I
41	631.14	4.32	631.19±0.03	1.49±0.23	631.28±16.01	631.19±2.33	Fe I
42	635.88	3.16	635.99±0.04	1.99±0.33	636.00±16.33	635.61±9.93	Fe I
43	638.41	3.16	638.33±0.05	3.34±2.30	638.25±1868.45	638.16±63.88	Fe II
44	640.62	3.41	640.57±0.07	1.47±0.68	640.57±32911.04	640.38±115.27	Fe I
45	648.17	3.50	648.38±0.08	1.10±0.51	648.64±518.41	648.40±29.72	Fe I
46	667.90	4.06	667.87±0.08	1.17±0.41	667.81±81407.41	667.52±396.17	Fe I
47	675.36	4.89	675.57±0.11	1.11±0.50	675.53±7.59	675.24±19.02	Fe I
48	685.28	5.34	685.27±0.27	0.79±0.42	685.31±20472927.80	685.24±166.85	Fe I

Note: Welding parameters: welding current I=130 A, arc voltage U=18 V, Ar + CO_2 as a shielding gas.

increases proportionally the probability of collisions among atoms and decreases the time that the atom remains in an excited state. It thus broadens the line width, because this is the quantum mechanical analog of damping to a classical oscillator. The Doppler broadening is caused by the very high temperature of the order of tens of thousands of degrees Kelvin of the arc plasma. This very high temperature increases proportionally the average speed of the atoms and, therefore, the Doppler shifts of the line either by molecules that move toward or away from the spectrophotometer is considerable (Ref. 46).

In the recorded spectrum of the welding arc light emission, separation of the iron and manganium atomic lines is possible (Table 4). The correlation between the intensity of the visible arc radiation and welding current is obtained. An increase in the welding current results in the intensity increase of the selected spectral line of the GMAW arc radiation — Fig. 6. Three fitting functions — Lorentz, Gauss, and Voight — were investigated as the methods to simulate the spectrum distribution.

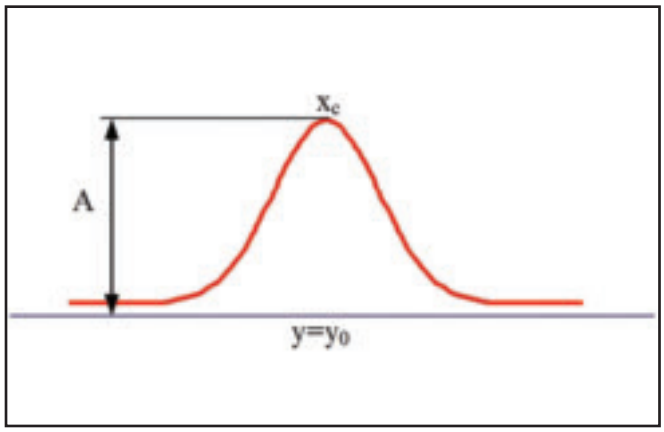

Fig. 9 — Characteristic qualities for the Voight function.

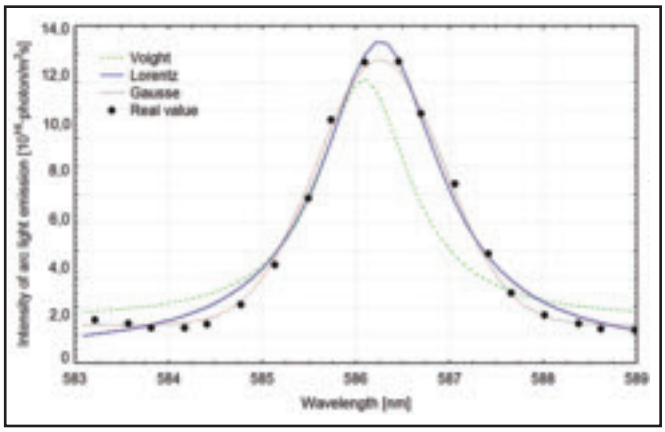

Fig. 10 — Calculated line profile of the wavelength 586.27 nm compared with measured values. The Gaussian, Lorentz, and Voight functions.

A very small difference between real wavelength and Lorentz model (Table 4) indicates that the best result can be obtained by the Lorentz function. The Gauss and Voight functions cannot be used to appropriately simulate the shape of each wavelength in the GMAW arc.

Conclusions and Future Work

The spectra of the radiation in the range of 480–700 nm of the welding arc in GMAW were analyzed. The following conclusions can be drawn from the investigation:

1. The main source of arc light radiation in GMAW is liquid metal. The major metallic lines identified were Fe I, Fe II, Fe III, Fe IV, Fe XVI, Fe XXI, and Mn I, Mn XIX and Mn XX. The lines from shielding gases weren't found.

2. An increase in the welding current results in the intensity increase of the selected spectral line of the welding arc radiation in GMAW.

3. The Lorentz function provided the best result from the simulation of the spectrum distribution of welding arc light radiation in GMAW. Small differences between real wavelength and the Lorentz model were observed.

The experience gained during these investigations allows further research on the welding arc radiation phenomenon. The obtained knowledge increases the possibilities of using the signal for online monitoring of the welding process on automated and robotized stands. The analysis of the spectrum of the radiation of the welding arc helps to develop a new vision sensor for arc welding.

Further work is planned in the following areas:

- Finding the correlation between the intensity of the visible arc radiation and other welding parameters, and disturbances of the welding process,
- Image processing to compare the modes of transfer metal in GMAW process with arc light emission,
- Utilizing these methods for monitoring the laser welding process on the robotic stand,
- Neural network and fuzzy process control.

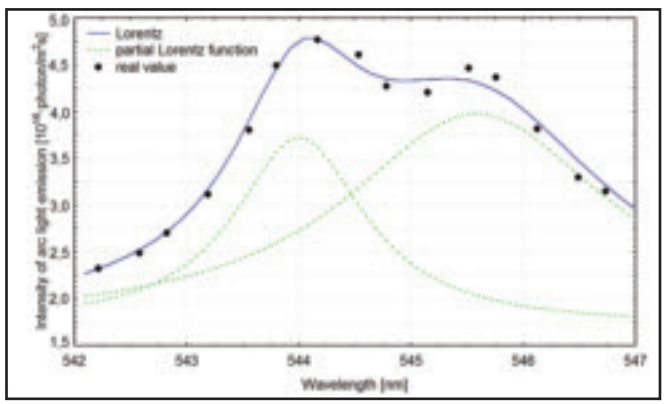

Fig. 11 — The calculated line profiles of wavelengths 544.0 and 545.68 nm were compared with measured values. The Lorentz function and the partial Lorentz function are presented.

Acknowledgments

The author would like to express his appreciation to Prof. Marian Nowak and Mirosława Kepińska, PhD, from the Solid State Physics Deparment at the Silesian University of Technology (Poland) for their support during the course of this research. The work described in this paper was partially supported by the Polish Ministry of Education and Science under Grant 3 T10C 021 28. The author would like also to thank the Fulbright Commission for partially financing this research, which was done within the framework of the research project Young Advanced Research Grant 2007-2008.

References

1. Messler, R. W. 1999. *Principles of Welding, Processes, Physics, Chemistry, and Meallurgy,* Chapter 3. pp. 60–66, New York, N.Y.: John Wiley & Sons.

2. Blakeley, P. J. 1990. Who should be using arc monitoring? *Welding and Metal Fabrication* 58(6): 268–272.

3. Siewert, T., and Madigan, B. 1992. Through the arc sensing for measurement of gas metal arc weld quality in real time. *Materials Evaluation* 50(11): 1314–1318.

4. Chen, X. Q. 2002. *Advanced Automation Techniques in Adaptive Material Processing*. pp. 125–166, New Jersey, Word Scientific Publishing.

5. Pan, J. 2003. *Arc Welding Control*. pp. 85–88, Cambridge, UK: Woodhead Publisher Ltd.

6. Zhang, Y. M. 2007. *Real Time Monitoring of Welding Processes.* Cambridge, UK: Woodhead Publisher Ltd.

7. Luksa, K. 1999. Monitoring of welding processes. *Bulletin of Welding Institute* 43(5): 59–62 (in Polish).

8. Weglowski, M. S. 2006. Utilization of arc light emission to control of welding process. *Bulletin of Welding Institute* 50(6): 43–48 (in Polish).

9. Kim, J. W., and Na, S. J. 1991. A study on an arc sensor for gas metal arc welding of horizontal fillets. *Welding Journal* 70(8): 216-s to 221-s.

10. Johnson, J. A., Carlson, N. M., Smartt, H. B., and Clark, D. E. 1991. Process control of GMAW: Sensing of metal transfer mode. *Welding Journal* 70(4): 91-s to 99-s.

11. Modenesi, P. J., and Nixon, J. H. 1994. Arc instability phenomena in GMA welding. *Welding Journal* 73(9): 219-s to 224-s.

12. Luksa, K. 2006. Influence of weld imperfection on short circuit GMA welding arc stability. *Journal of Materials Processing Technology* 175(1-3): 285 to 290.

13. Guu, A. C., and Rokhlin, S. I. 1992. Arc welding process control using radiographic sensing. *Materials Evaluation* 50(11):

1344–1348.

14. Fan, H., Ravala, N. K., Wikle III, H. C., and Chin, B. A. 2003. Low-cost infrared sensing system for monitoring the welding process in the presence of plate inclination angle. *Journal of Materials Processing Technology* 140(1-3): 668–675.

15. Carlson, N. M., and Johnson, J. A. 1992. Ultrasonic NDT methods for weld sensing. *Materials Evaluation* 50(11): 1338–1343.

16. Taylor-Burge, K. L., and Harris, T. J. 1993. The real time analysis of acoustic weld emission using neural networks, *Proc. of the International Conf. on the Joining of Materials JOM-6 ed*. Rasmus Knudsens Vej, pp. 60-67. Ingeniorhojskolen Helsingor Teknikum, Denmark.

17. Saini, D., and Floyd, S. 1998. An investigation of gas metal arc welding sound signature for on-line quality control. *Welding Journal* 77(4): 172-s to 179-s.

18. Luksa, K. 2003. Correspondence between sound emission generated in GMA (MIG/MAG) welding process and signals registered in the arc circuit. *Welding International* 17(6): 438–441.

19. Smith, J., and Lucas, B. 1999. Putting intelligence into welding — Rule based systems, fuzzy logic and neural networks. *Welding & Metal Fabrication* 67(10): 7–9.

20. Wu, C. S., Polte, T., and Rehfeldt, D. 2001. A fuzzy logic system for process monitoring and quality evaluation in GMAW. *Welding Journal* 80(2): 33-s to 38-s.

21. Hermans, J. M., and Den Ouden, G. 1999. Process behavior and stability in short circuit gas metal arc welding. *Welding Journal* 78 (4): 137-s to 141-s.

22. Chu, Y. X., Hu, S. J., Hou, W. K., Wang, P. C., and Marin, S. P. 2004. Signature analysis for quality monitoring in short circuit GMAW. *Welding Journal* 83(12): 336-s to 343-s.

23. Amin, M., and Naseer, A. 1987. Synergic control in MIG welding — Parametric relationship for steady DC open arc and short circuiting arc operation. *Metal Construction* 19(1): 22–28.

24. Kang, Y. H., and Na, S. J. 2003. Characteristics of welding and arc signal in narrow groove GMAW using electromagnetic arc oscillation. *Welding Journal* 82(5): 93-s to 99-s.

25. Lu, W., and Zhang, Y. M. 2004. Sensing of weld pool surface using nontransferred plasma charge sensor. *Measurement Science and Technology* 15(5): 991–999.

26. Zheng, B., and Wang, H. J. 2000. Control for weld penetration in VPPAW of aluminum alloys using the front weld pool image signal. *Welding Journal* 70(12): 363-s to 371-s.

27. Smith, J. S., and Balfour, C. 2005. Vision sensor in arc welding. *Document International Institute of Welding* MIS XII-1850-05.

28. Zhang, Y. M., and Wu, L. 1993. Determination of joint penetration in GTAW with vision sensing of weld face geometry. *Welding Journal* 72(10): 463-s to 469-s.

29. Kim, E. W., Allemand, C., and Eagar, T. W. 1987. Visible light emission during gas tungsten arc welding and its application to weld image improvement. *Welding Journal* 66(12): 369-s to 377-s.

30. Li, P. J., and Zhang, Y. M. 2001. Precision sensing of arc length in GTAW based on arc light spectrum. *Journal of Manufacturing Science and Engineering* 123(1): 62–65.

31. Weglowski, M. S. 2005. Sensing of arc length in the TIG welding method based on arc light intensity. *Advances in Manufacturing Science and Technology* 29(2): 31–41.

32. Li, P. J., and Zhang, Y. M. 2000. Analysis of an arc light mechanism and its application in sensing of the GTAW process. *Welding Journal* 79(9): 252-s to 260-s.

33. Wang, Q. L., and Li, P. J. 1997. Arc light sensing of droplet transfer and its analysis in pulsed GMAW processes. *Welding Journal* 76(11): 458-s to 469-s.

34. Weglowski, M. S. 2007. Utilization of the arc light emission emitted during TIG welding to monitoring this process. *Archives of Mechanical Technology and Automation PAN* 27(1): 103–112 (in Polish).

35. Yoo, C. D., Yoo, Y. S., and Sunwoo, H. K. 1997. Investigation on arc light intensity in gas metal arc welding. Part 1: Relationship between arc light intensity and arc length. *Proceeding of the Institution of Mechanical Engineers. Part B: Journal of Engineering Manufacture* 211(B5): 345–353.

36. Yoo, C. D., Yoo, Y. S., and Sunwoo H. K. 1997. Investigation on arc light intensity in gas metal arc welding. Part 2: Application to weld seam tracking. *Proceeding of the Institution of Mechanical Engineers. Part B: Journal of Engineering Manufacture* 211(B5): 355–363.

37. Ancona, A., Lugarà, P. M., Ottonelli, F., and Catalano, I. M. 2004. A sensing torch for on-line monitoring of the gas tungsten arc welding process of steel pipes. *Measurement Science and Technology* 15(12): 2412–2418.

38. Hinrichs, J. F. 1978. Radiation and arc welding: New data to enhance safety. *Welding and Metal Fabrication* 51(2): 102, 103.

39. Pattee, H. E., Myers, L. B., Evans, R. M., and Monroe, R. E. 1973. Effect of arc radiation and heat on welders. *Welding Journal* 52(5): 297–308.

40. Kohmoto, K. 1992. Variation of degree of blue light hazardous damage by the crystalline lens deterioration. *Document International Institute of Welding* MIS VIII-1630-92.

41. Weglowski, M. 2005. Determination of GTA and GMA welding arc temperature. *Welding International* 19(3): 186–192.

42. Inoue, K. 1981. Image processing for online detection of welding process (Report III) — Improvement of image quality by incorporation of spectrum of arc. *Transaction of JWRI* 10(1): 13–18.

43. Database of wavelength NIST: *http://physics.nist.gov/cgibin/AtData/lines_form.*

44. Zielińska, S. 2004. Physical properties of plasma MIG-MAG. PhD dissertation. Krakow (Poland), Krakow University of Technology (in Polish).

45. Database of wavelength- *http://riodb.ibase.aist.go.jp/rfp_db/waveleng/index.html.*

46. Agapiou, G., and Kasiouras, C. 1999. A detailed analysis of the MIG spectrum for the development of laser-based seam tracking sensor. *Optics & Laser Technology* 31(2): 157–161.